

Cyclic Oxidation of P91 by Thermogravimetry and Investigation of Integrity of Scale by “Transient-Mass-Gain” Method

S. Rajendran Pillai · R. K. Dayal

Received: 24 May 2007 / Revised: 10 October 2007 / Published online: 8 January 2008
© Springer Science+Business Media, LLC 2008

Abstract The growth and degradation of the oxide scale on modified 9Cr–1Mo ferritic steel was studied at 1123 K using a thermogravimetric balance by employing the “transient-mass-gain method” in conjunction with the adaptation of a cyclic-oxidation procedure. The total duration of the oxidation was 1000 h. The experiment revealed that the cracking of the scale was initiated when the average thickness was 72 μm . Spallation occurred when the average thickness was 75 μm . The rate of spallation was found to be enhanced as the scale thickens and attained a higher rate after 90 μm . The rate constants for the different stages of oxidation were found to be different. The specimen was examined by SEM, EDS and XRD. The scale morphology revealed outwardly protruded growth, a uniform adherent oxide layer and a spalled region. Four oxide phases were identified; Cr_2O_3 , Fe_2O_3 , $(\text{FeCr})_2\text{O}_3$ and FeCr_2O_4 . The spall contained more $(\text{FeCr})_2\text{O}_3$ whereas the adherent scale was more FeCr_2O_4 .

Keywords Cyclic oxidation · Scale failure · P91 steel · Transient-mass-gain method

Introduction

It is necessary for high-temperature components to have predictable and economically viable life times. Moreover, the thickness of components has to be kept at an optimum level so that process efficiency is not compromised. In this context, the development of a slowest growing and protective scale on the surface assumes extreme importance. Such a scale is capable of protecting the underlying alloy from

S. Rajendran Pillai (✉) · R. K. Dayal
Corrosion Science and Technology Division, Indira Gandhi Centre for Atomic Research,
Kalpakkam, Tamil Nadu, India 603 102
e-mail: srp@igcar.gov.in

further oxidation. Hence an important consideration for the selection of material for high-temperature service is the capacity to form a protective scale under varying conditions of stress and environmental parameters [1–4]. The factors limiting the life of the oxide scale and the possible means to achieve better adherence have been discussed in the literature [5, 6].

Ferritic steel, a modified 9Cr–1Mo steel (commercially called P91) finds application in high-temperature steam/water environment because of its favorable mechanical properties coupled with good resistance to water-induced stress–corrosion cracking. In fast reactors, this alloy is employed in the fabrication of steam generator and decay-heat-removal systems. One of the major limitations of this alloy is its susceptibility to oxidation and the consequent loss in thickness of the components. The adhering oxides also impair the heat-transfer characteristics. Among the constituents, chromium forms a thermodynamically more-stable oxide than the other elements. However, the concentration of chromium required to form the protective scale is in the range of 16–20 mass% for temperatures in the range of 873–1273 K [7, 8]. This higher concentration, at least in principle, could be achieved at the surface by diffusion followed by simultaneous oxidation. However, iron has a higher diffusion rate than chromium through the pre-existing scale [9]. As a consequence, the oxide scale generated on the surface may contain iron as the major constituent. Oxides of iron have poor adherence properties when compared to chromium oxide. Chromium oxide also suffers spallation, though to a reduced extent when compared to iron oxide, especially when reactive elements are not added to the alloy.

The growth and the progress of thickening of the oxide scale on an alloy such as modified 9Cr–1Mo ferritic steel under thermal-cycling conditions is expected to proceed in different steps, as envisaged from data reported in the literature [1–6]. If the integrity of the oxide scale is good, then after the formation of an initial layer, further growth is controlled by a diffusion-controlled process (parabolic rate law). As the thickness increases, the growth rate slows down. The second stage of oxidation starts when the thickness of the scale has attained a critical value. At this point, the scale starts developing cracks. This results in exposure of fresh surface to oxidation. The crack may be healed almost instantaneously. The rate of oxidation is expected to be enhanced due to the exposure of fresh surface at periodic intervals. The instantaneous cracking and healing would manifest as though the oxide scale is accommodating a large thermal strain without any loss in integrity [10, 11].

In the third stage the rate of cracking is faster than the process of healing. Thus, fresher surface will be exposed to oxidation for longer times. As a result the scale grows at a faster rate. If the alloy is subjected to oxidation for a longer duration, the scale thickness increases to a value higher than a critical limit and spallation occurs. This is the fourth stage, wherein the alloy undergoes an accelerated loss in wall thickness. This is a life-limiting situation, because if it is allowed to continue for a long time the load bearing capacity of the component would be impaired, ultimately leading to failure [12].

There is a fifth stage of catastrophic oxidation likely to be encountered in the case of some alloys due to repeated spallation. In certain alloys, the generation of

a protective scale is achieved by the addition of one or more special elements such as silicon or aluminum. These elements are capable of diffusing faster and generating a scale with good stability and adherence at the surface. Repeated spallation of the scale due to thermal cycling would lead to depletion of the elements which are responsible for the generation of an adherent scale by preferentially diffusing into the surface. As a consequence, the capacity of the alloy to form a protective scale is impaired, and the alloy enters a stage called catastrophic oxidation [13–16]. In this situation the loss in wall thickness would be very fast, and failure of the component is imminent. Krupp et al. [17] reported yet another reason for the adverse impact on mechanical properties due to oxidation. These authors examined the process of internal corrosion by a numerical model on a nickel-base alloy, Nicrofer 7520 Ti and found evidence for internal oxidation affecting mechanical properties.

The development of wedge-type cracks and instantaneous healing has been reported in the literature [10, 11] during isothermal oxidation. The macroscopic integrity of the scale will not be disturbed during this process. Each cracking will be associated with instantaneous healing. The thermal expansion of the matrix will be largely accommodated by the constant cracking and instantaneous healing processes. Thus, even a ceramic oxide scale appears to accommodate a large strain. In other words the occurrence of cracking followed by instantaneous healing is not detectable. This phenomenon is called ‘pseudoplasticity’ [2]. As a consequence of this process the adherence of the scale tends to improve by accommodating growth stress. On the other hand during the cooling stage, encountered in the case of cyclic oxidation, the oxide scale experiences a compressive stress, because the thermal-expansion coefficient of alloys is always higher than the corresponding oxides. When the thickness of the scale is above a critical value, the compressive stress is adequate to cause wedge-type cracks or to develop buckling followed by spallation [11].

Among the major constituents of P91, chromium forms the most-stable oxide. But the predominant oxide phase at the surface is that of iron on account of its high rate of diffusion [9, 18, 19]. The present study is aimed at determining the critical thickness of the oxide scale on P91 corresponding to the different stages of oxidation discussed above. The last stage of catastrophic oxidation is not expected to be encountered in this alloy.

Experimental Procedures

Specimen Preparation

The composition of the alloy employed is given in Table 1. The specimen was cut into approximately $15 \times 10 \times 3$ mm size and given a heat treatment similar to the welded components. It was carried out by heating at 1353 K for 1 h followed by 1013 K for 1 h. In both cases the specimen was cooled in the furnace to room temperature. This specimen was polished using successive grades of polishing paper to obtain a surface finish of 5 μm .

Table 1 Chemical composition of P91

| Element | Cr | Mo | V | Ni | Nb | Mn | Ti | C | P | Cu | Al | Si |
|---------|-----|-----|------|------|-------|-----|-----|-----|-------|-----|-----|------|
| Content | 8.7 | 0.9 | 0.15 | 0.03 | 0.046 | 0.4 | <10 | 160 | 0.029 | 160 | 230 | 0.32 |

Note: The contents of C, Ti, Cu and Al are expressed in PPM. Other elements are expressed in mass%. The balance is iron

Thermogravimetric Analysis: “Transient-Mass-Gain Method”

The behavior of oxide scales has been studied by several investigators by employing the cyclic-oxidation method [20–23]. However, these involve discontinuous experiments. Samples are removed at select intervals from the furnace to determine the mass change by weighing in a balance. In this method two experimental options are available; hang the sample freely inside the furnace or hold in a crucible. In the former case, only net mass gain is available which may not be adequate for a complete description of the process. In the latter case, the total mass gain which includes that of the spall is obtained. The limitations of both these methods are comprehensively discussed in the literature [24].

Keeping these problems in mind few authors have attempted a continuous thermogravimetry for cyclic oxidation [24–29]. Monceau and Poquillon [24] have employed equipment built by Salabura and Monceau [30] that can offer very high heating and cooling rates of 823 K/min. Thus, the mass gain in the heating and cooling duration may be neglected. Raffaitin et al. [29] applied a cyclic-oxidation analysis to examine the influence of MCrAlYTa (where M = Ni, Co) coating on a nickel-base superalloy. The study clearly established the beneficial effects of a coating in improving the cyclic-oxidation resistance without decreasing the isothermal-oxidation kinetics. A similar experiment was carried out in the present study using a thermobalance.

A thermogravimetric balance (Model Setsys 12, M/s Setaram, France) was employed in the investigation. This balance has a sensitivity of 0.4 μg and a resolution of 0.04 μg . The accuracy of the balance is $\pm 0.5 \mu\text{g}$. The integrity of the oxide scale was monitored by “transient-mass-gain” method which is analogous to the cyclic thermogravimetry reported by Monceau and Poquillon [24]. This method is based on the premises that a disturbance to the integrity of the oxide scale that has already formed, in the form of a crack, buckling or spallation results in exposure of fresh surface and an instantaneous mass increase by oxidation. The mass gain associated with such a process is expected to be very small (of the order of 0.1 μg). However, the thermogravimetric balance employed in the present investigation has adequate resolution to detect this small gain in mass. The failure of the scale is indicated as a small hump in the thermogram. The transient-mass-gain is taken only as a qualitative indication of the integrity of the scale.

The buoyancy effect was corrected by running blank experiments. The mass increase in the isothermal-hold period was taken in all the calculations. The mass gain during the heating and cooling ramps has been evaluated to contribute less than

0.5% in the total mass gain and therefore was neglected. The mass gain was accessed using software called Setsoft (Supplied by M/s Setaram, France) in the real-time mode.

Before starting the experiment with the specimen, a blank run was carried out to check the satisfactory performance of the weighing module. Absence of a drift (implying mass gain below the detection limit) in the thermogram for the desired experimental duration was taken as the indication of satisfactory performance of the analyzer. The specimen was introduced into the platinum crucible, and the oxidation experiment was carried out under the following conditions;

Heating rate: 30 K/min

Temperature of oxidation: 1123 K

Isothermal-retention period: 2 h for 110 cycles (220 h) and subsequently 5 h up to 268 cycles (1000 h)

Cooling rate: 20 K/min

The experimental procedure enabled the determination of total mass gain and the spall mass retained in the crucible separately.

The possibility of an error due to the evaporation of PtO₂ was precluded at the present temperature. Based on data in the literature [31, 32], it was evaluated that the mass loss at 1123 K for 1000 h is less than 0.5% of the corresponding mass gain due to oxidation of the specimen.

The chosen temperature of investigation is higher than the normal application range of the alloy and it is known to undergo a phase change at this temperature. However, this temperature is chosen based on experience gained in an earlier study [4] coupled with factors such as necessity to get measurable oxide growth. The experiment attempts to drive home the philosophy of generation, growth and destruction of oxide scale on a commercial alloy.

The specimen was held in a platinum crucible and lowered into the hot zone of the vertical furnace attached to the thermogravimetric balance. The mass gain associated with each cycle was individually determined by the thermogravimetric method. At the end of each cycle, the specimen was taken out, and masses of crucible with and without the specimen were determined by using a balance having a sensitivity and accuracy of ± 0.1 mg. Thus, the mass of the spalled oxide, which was retained in the platinum crucible, was also determined at the end of each cycle (all the 268 cycles).

From the mass gain-data obtained by thermogravimetry, the mass of the oxide was calculated by assuming that oxidation reaction is,



where M is a combination of chromium and iron. In this calculation, the relative proportion of metal in the oxide was assumed to be same as that in the basic alloy. It is evident that the metal fraction of the oxide is not same as that in the base metal, especially as oxidation proceeds. However, this assumption is not expected to introduce a significant deviation from the actual value as the atomic masses of chromium and iron are not significantly different.

$$\sum_n \text{mass of adherent scale} = \sum_n \text{cumulative mass gain of oxide} - \sum_n \text{mass of spall.} \quad (2)$$

$$\frac{\sum_n \text{mass of adherent scale}}{\text{Density of oxide} \times \text{surface area of specimen}} = \text{thickness} \quad (3)$$

where n is the number of cycles of oxidation. The density of oxide is taken as average of Fe_2O_3 and Cr_2O_3 which is $5.23 \times 10^3 \text{ kg m}^{-3}$ [33]. The surface area of the specimen was 184.6 mm^2 . The mass gain due to oxidation (oxygen in take) is multiplied by 3.3125 (the atomic mass ratio of M_2O_3 to O_3 in $(\text{FeCr})_2\text{O}_3$) to convert to oxide equivalent based on the formation reaction given by Eq. 1. The thicknesses corresponding to various stages of scale behavior such as cracking, spallation and enhanced spallation were evaluated using Eq. 3.

The rate of increase in mass due to oxidation is given by,

$$\frac{dx}{dt} = \frac{k'_p}{x} \quad (4)$$

where

$$x = \text{Mass gain in mg mm}^{-2}$$

$$t = \text{time in seconds}$$

Integrating Eq. 4 between time limits 0 to t when the mass varies from 0 to x ;

$$x^2 = 2k'_p t \quad (5)$$

$$x^2 = k_p t \quad (6)$$

where $k_p = 2k'_p$; k_p is the parabolic rate constant expressed in $\text{mg}^2\text{mm}^{-4}\text{s}^{-1}$

Results and Discussion

Genesis of Oxide Scale and the Determination of Rate Constants

Each stage of oxidation is governed by different kinetics. Hence, evaluation of corrosion loss based on a single rate constant would lead to inaccurate prediction of life of components. The gain in mass of the specimen due to oxidation and the cumulative mass of spall are given in Fig. 1. The mass gain represented the intake of oxygen whereas the mass of spall is that of the oxide.

The parabolic rate constants were evaluated corresponding to each cycle and are shown in Fig. 2. In order to determine the parabolic rate constant, the mass gain in each cycle was determined from the thermogram and while calculating the thickness it was converted to corresponding oxide. The rate constant was calculated by employing Eq. 6. At each cracking and spallation, fresh surface is exposed to oxidation, and therefore the rate constant is bound to change. Thus, the calculated k_p

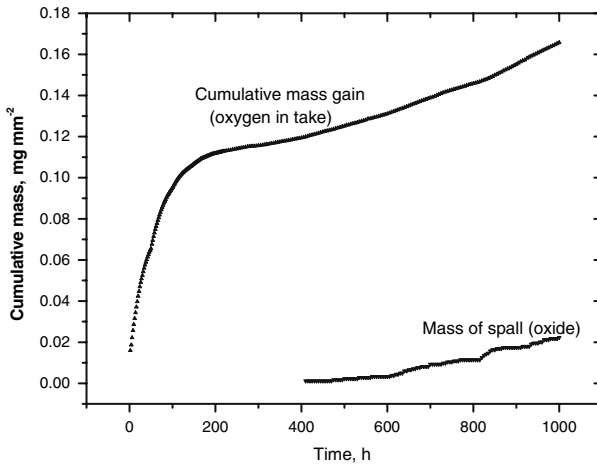


Fig. 1 Cumulative mass gain and the mass of spall at different duration

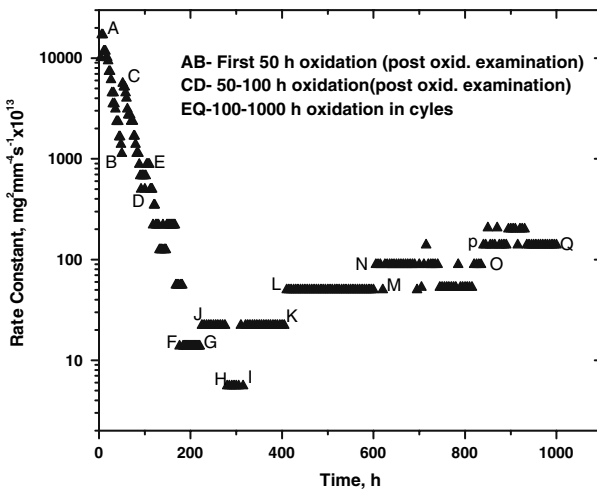


Fig. 2 Variation of parabolic rate constants with cycles of oxidation (up to 220 h, 2 h cycles. 220–1000 h, 5 h cycles)

is more appropriately an apparent value. The initial rate was relatively high and decreased rapidly and reached a lowest value after 70 h. The initial rapid rate is attributed to two factors,

- (a) Exposure of the freshly polished surface leads to the oxidation rate being governed by the linear law. Once a uniform oxide layer has been formed, further oxidation proceeds by the parabolic rate law governed by diffusion.
- (b) The thickness of the initially formed layer is very small (nearly 10 μm) through which ions of chromium and iron can diffuse fast enough to contribute to the thickening of the scale.

As the thickness of the scale increases, the time of diffusion through the pre-existing scale is increased so that oxidation proceeds at a very slow pace. However, at higher thickness beyond a critical value, the oxide scale undergoes cracking, especially on cooling, resulting in an enhanced rate of oxidation. In the present investigation, the scale has attained a thickness of 72 μm after oxidation for 270 h. At this juncture; the scale indicated development of cracking, indicted by a small gain in mass. This thickness is the threshold value for the development of cracks. Cracking was observed periodically in subsequent cycles also. The healing of the cracks contributed to successive steps of increase in the parabolic rate constant.

On cooling, after oxidizing for 410 h the first sign of spallation was noticed. It became evident when the crucible was weighed at the end of the experiment after removing the specimen wherein a mass increase was observed. At the initiation of spallation the thickness of the scale was 75 μm . The extent of spallation increased in successive cycles. An accelerated rate of spallation was noticed after 820 h when the thickness of the scale was 90 μm .

An SEM micrograph of the oxidized specimen is shown in Fig. 3. The figure clearly shows four distinct regions which corroborate the anticipated scale behavior. The distinct regions are;

- (i) Region of adherent scale
- (ii) Region of protruded (outward) oxide growth
- (iii) Wedge-type crack formation
- (iv) A spalled region with formation of a new oxide layer

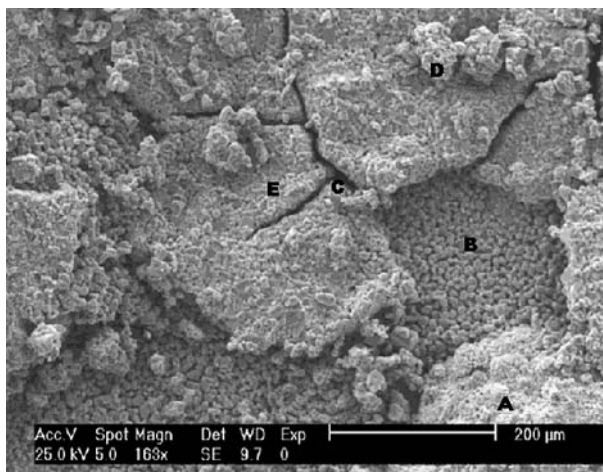


Fig. 3 SEM micrograph of the surface oxidized for 1000 h. The different regions marked on the micrograph are (A and E) Adherent regions (B) Inside scale of spalled region (C) Wedge type cracking of the scale (D) Outgrowth of the scale

The microscopic examination was carried out only at the end of the experiment as the scale formed was sensitive to the rigors of handling in an SEM system.

Chemical Analysis of Oxidized Surface

The different locations marked on the SEM micrographs have been analyzed by Energy-Dispersive Spectrometry. The results are given in Table 2.

The adherent scale region (A and E in the micrograph) showed a relatively higher concentration of iron (93–95 mass%). The concentration of chromium was in the range of 5–7 mass%. The concentration of silicon in the scale was below the limit of detection. On the other hand the porous outgrowth showed the presence of silicon and enhancement in the concentration of chromium. This region presumably represents a grain boundary where the diffusion of silicon and chromium are also as fast as that of iron. The fraction of chromium oxide in the scale was higher because it is thermodynamically more stable than the oxide of iron.

The cracked interspaces (wedge region) revealed an increase in the concentration of chromium. This is due to enhanced diffusion of cations through the cracks. Thus, the relatively slow-diffusing chromium also reaches the crack tip and gets oxidized.

As a result of spallation, the interspace of the oxide-metal was exposed to fresh oxidation. In this region there was significant enhancement in the concentration of silicon and chromium. Both these elements are known to stifle the growth rate of oxide scale.

Characterization of Phases by XRD

The different oxide phases present in the spalled powder and retained on the surface revealed the presence of identical oxide phases; Cr_2O_3 , Fe_2O_3 , $(\text{Cr,Fe})_2\text{O}_3$ and FeCr_2O_4 . The spall contained more of the mixed oxide, $(\text{Cr,Fe})_2\text{O}_3$, whereas the adherent oxide on the specimen contained more of the spinel oxide, FeCr_2O_4 (Figs. 4 and 5).

Table 2 Chemical analysis by EDS of the different regions (ref. Fig. 3)

| Region | Composition, mass% |
|---|-----------------------------------|
| Porous outgrowth (region D in Fig. 3) | Si = 0.37; Cr = 12.31; Fe = 87.32 |
| Adherent scale (region E in the Fig. 3) | Si = LD; Cr = 7.42; Fe = 92.58 |
| (region A in the Fig. 3) | Si = LD; Cr = 4.91; Fe = 95.09 |
| Inside layer of spalled region (region B in Fig. 3) | Si = 1.3; Cr = 14.87; Fe = 83.83 |
| Cracked interspaces (region C in Fig. 3) | Si = LD; Cr = 11.11; Fe = 88.89 |

LD indicates less than detection limit

Note: The mass percentages of constituent elements were calculated by normalizing to a total content of 100%, ignoring oxygen

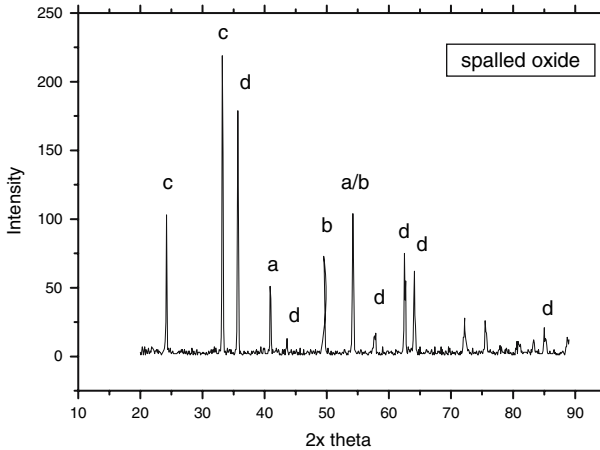


Fig. 4 XRD pattern of spalled oxide (a) Cr_2O_3 , (b) Fe_2O_3 , (c) $(\text{Cr,Fe})_2\text{O}_3$ (d) FeCr_2O_4

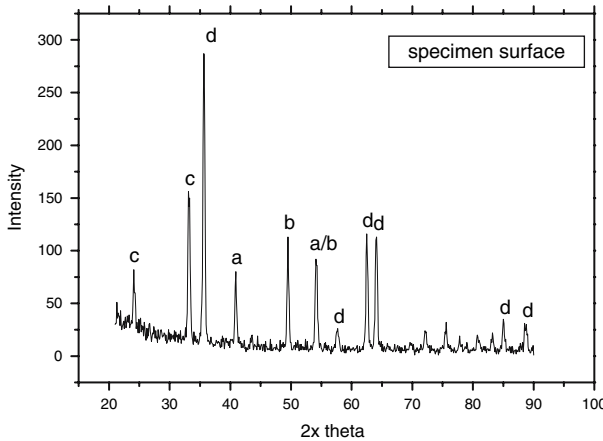


Fig. 5 XRD pattern of the oxide retained on the surface of the oxidized specimen (a) Cr_2O_3 , (b) Fe_2O_3 , (c) $(\text{Cr,Fe})_2\text{O}_3$ (d) FeCr_2O_4

Conclusion

1. The experiment sheds light on the different stages of scale failure.
 - Cracking of the scale occurred when the thickness was $72\ \mu\text{m}$
 - Spallation was initiated after the scale attained a thickness of $75\ \mu\text{m}$
 - Accelerated spallation was noticed on further thickening of scale and reached a high value when the scale thickness was $90\ \mu\text{m}$
2. The rate of spallation was found to increase as the thickness of the scale increases. This sheds light on the need to operate the components even without the onset of first spallation.

3. The region of catastrophic failure is not likely to be encountered by P91 as this material is not alloyed with enough chromium to selectively diffuse and form a truly protective scale.
4. The method of evaluating scale thickness and material wastage based on parabolic rate constants is not expected to provide a realistic estimation. The apparent rate constant itself increases with duration and progress of each thermal cycle.
5. Four oxide phases were found to be present in the spalled oxide and the adherent layer. These are Cr_2O_3 , Fe_2O_3 , $(\text{Cr,Fe})_2\text{O}_3$ and FeCr_2O_4 . The spall contained more $(\text{Cr,Fe})_2\text{O}_3$ whereas the adherent scale had more FeCr_2O_4 .
6. The outgrowths, presumably from the grain boundary regions, were enriched in chromium. This is attributed to the high rate of diffusion of chromium through fast-diffusion channels.

Acknowledgements The authors wish to acknowledge the help rendered by Mrs. M. Radhika, Physical Metallurgy Section, Materials Characterization Group, in SEM and EDS analyses and Mrs. S. Kalavathy, Materials Science Division in the XRD characterization.

References

1. N. J. Simms and J. E. Oakey, *Materials at High Temperatures* **13**(2), 75 (1995).
2. M. Schuetze, *Oxidation of Metals* **24**(3/4), 199 (1985).
3. H. E. Evans and R. C. Lobb, *Corrosion Science* **24**(3), 209 (1984).
4. S. Rajendran Pillai, P. Shankar, and H. S. Khatak, *High Temperature Materials and Processes* **23**(3), 196 (2004).
5. S. Rajendran Pillai, *Corrosion Reviews* **23**(4–6), 277 (2005).
6. W. J. Quadakkers and K. Bongartz, *Werkstoffe und Korrosion-Materials and Corrosion* **45**, 232 (1994).
7. R. Hales, *Werkstoffe und Korrosion-Materials and Corrosion* **29**, 939 (1978).
8. G. C. Wood, M. G. Hobby, and B. Vaszko, *Journal of the Iron and Steel Institute* **202**, 685 (1964).
9. C. Lille and R. F. A. Jargelius-Petersson, *Materials at High Temperatures* **17**(2), 287 (2000).
10. M. Schuetze, *Materials Science and Technology* **6**, 32 (1990).
11. S. Rajendran Pillai, N. Sivai Barasi, and H. S. Khatak, *Oxidation of Metals* **54**(3/4), 211 (2000).
12. H. E. Evans, G. P. Mitchel, R. C. Lobb, and D. R. J. Owen, *Proceedings of the Royal Society of London Series A* **440**(1908), 1 (1993).
13. T. Ohashi and T. Harada, *Oxidation of Metals* **46**(3/4), 235 (1996).
14. V. V. Belousov and B. S. Bokshstein, *Oxidation of Metals* **50**(5/6), 389 (1998).
15. F. J. Perez, F. Pedraza, M. P. Hierro, J. Balmain, and G. Bonnet, *Surface and Coatings Technology* **153**(1), 49 (2002).
16. L. Mikkelsan and S. Linderorth, *Materials Science and Engineering A* **361**(1/2), 198 (2003).
17. U. Krupp, S. Y. Chang, A. Schimke, and H.-J. Christ, in *Lifetime Modelling of High Temperature Corrosion Processes*. M. Schuetze, W. J. Quadakkers, and J. R. Nicholls, eds. (EFC 34, Maney Publishing, London, 2001), p. 148.
18. A. F. Smith, *Corrosion Science* **21**(7), 517 (1981).
19. S. N. Basu and G. J. Yurek, *Oxidation of Metals* **36**(3/4), 281 (1991).
20. M. Schuetze, *Oxidation of Metals* **44**, 29 (1995).
21. J. R. Nicholls and M. J. Bennett, in *Cyclic Oxidation of High Temperature Materials*. M. Schuetze and W. J. Quadakkers, eds. (IOM Communications Ltd., London, 1999), Vol. EFC 27, p. 437.
22. J. L. Smialek, J. A. Nesbitt, C. A. Barrett, and C. E. Lowell, Report NASA/TM-2000-209769.
23. J. R. Nichols and M. J. Bennett, *Materials at High Temperatures* **17**(3), 413 (2000).
24. D. Monceau and D. Poquillon, *Oxidation of Metals* **61**(1/2), 143 (2004).

25. J. C. Pivin, D. Delaunay, C. Roques-Carnes, A. M. Huntz, and P. Lacombe, *Corrosion Science* **20**, 351 (1980).
26. S. Y. Chang, U. Krupp, and H. J. Christ, in *Cyclic Oxidation of High Temperature Materials*. M. Schuetze and W. J. Quadackers, eds. (IOM Communications Ltd., London, 1999), Vol. EFC 27, p. 63.
27. P. Vangeli and B. Ivarsson, *Materials Science Forum* **369–372**, 785 (2001).
28. P. Vangeli, in *Cyclic Oxidation of High Temperature Materials*. M. Schuetze and W. J. Quadackers, eds. (IOM Communications Ltd., London, 1999), Vol. EFC 27, p. 198.
29. A. Raffaitin, D. Monceau, E. Andrieu, and F. Crabos, *Acta Materialia* **54**(17), 4473 (2006).
30. J.-C. Salabura and D. Monceau, *Materials Science Forum* **461–464**, 689 (2004).
31. J. Herman, *Journal of Less Common Metals* **100**, 321 (1984).
32. W. L. Phillips Jr., *Transactions of the American Society for Metals* **57**, 33 (1964).
33. D. R. Lide, *CRC Handbook of Chemistry and Physics*, 80th edn. (CRC Press, London, 1999–2000), p. 4.